Mapping the plasmon response of Ag nanoislands on graphite at 100 nm resolution with scanning probe energy loss spectroscopy

Murphy, Shane; Bauer, Karl; Sloan, Peter A.; Lawton, James J.; Tang, Lin; Palmer, Richard E.

DOI:
10.7567/APEX.8.126601

Mapping the plasmon response of Ag nanoislands on graphite at 100 nm resolution with scanning probe energy loss spectroscopy

2015 Appl. Phys. Express 8 126601

(http://iopscience.iop.org/1882-0786/8/12/126601)

OPEN ACCESS

Applied Physics Express 8, 126601 (2015)

http://dx.doi.org/10.7567/APEX.8.126601

Mapping the plasmon response of Ag nanoislands on graphite at 100 nm resolution with scanning probe energy loss spectroscopy

Shane Murphy, Karl Bauer, Peter A. Sloan, James J. Lawton, Lin Tang, and Richard E. Palmer

Nanoscale Physics Research Laboratory, School of Physics and Astronomy, University of Birmingham, Edgbaston, Birmingham B15 2TT, U.K.

Received October 12, 2015; accepted October 25, 2015; published online November 13, 2015

We demonstrate plasmon mapping of Ag nanostructures on graphite using scanning probe energy loss spectroscopy (SPELS) with a spatial resolution of 100 nm. In SPELS, an STM tip is used as a localized source of field-emitted electrons to probe the sample surface. The energy loss spectrum of the backscattered electrons is measured to provide a chemical signature of the surface under the tip. We acquire three images simultaneously with SPELS: i) constant-current field-emission images, which provide topographical information; ii) backscattered electron images, which display material contrast; and iii) SPELS images, where material-dependent features such as plasmons are mapped.

While scanning tunneling microscopy (STM) is an excellent tool for elucidating surface topographic and structural information with extraordinary detail, it is generally unsuitable for elemental identification owing to the fact that scanning tunneling spectroscopy (STS) probes valence electron states that are strongly perturbed by the local chemical environment. Consequently, there is a strong incentive to combine the high spatial resolution offered by STM with the type of spectroscopic information available from Auger electron spectroscopy (AES) or electron energy loss spectroscopy (EELS) measurements, both of which can be initiated by electron impact. This can be achieved by operating the STM in the field-emission regime to provide an highly localized source of primary electrons with which to probe a surface while using an energy-dispersive electron detector to measure the energies of the resulting backscattered and/or secondary electrons. By selecting an appropriate tip bias, it is possible to probe either valence or core states in order to yield a definitive chemical signature of the surface.

Spectroscopic measurements with a field-emission scanning probe microscope were first reported by Reihl and Gimzewski,[1] who obtained single-point AES and EELS spectra on oxidized silicon by using tip biases in the 500–1000 V range and tip–sample separations of several hundred micrometers. Further measurements have been reported by a number of groups on various surfaces such as graphite, silicon, and gold, which agree well with corresponding spectra measured using conventional AES and EELS.[2–7] Introducing angle-resolved measurements, Eves et al.[4] demonstrated that the angular distribution of the electrons scattered from the tip–sample region is maximized in the direction parallel to the sample surface owing to the strong repulsive field from the negatively biased tip. While the number of electrons impinging the surface is maximized directly below the tip apex, the number of backscattered electrons escaping from the tip–sample region is reduced to zero at the same position. As a consequence, the electrons scattered from the sample to the detector originate from a narrow annulus around the position of the STM tip.[5] The net effect is that the spatial resolution of the backscattered/secondary electron image is improved compared with that of the corresponding field-emission image. A best-case angle-resolved spatial resolution of the order of 1–10 nm has been estimated for a field-emission measurement with a resolution of 100 nm.[5] The energy resolution reported to date is of the order of 0.6 eV.[5] This is within the energy range of plasmon excitations and interband transitions, which can be used for chemical identification. Most previous studies have reported single-point or area-averaged measurements, and there have only been a few studies where spatially resolved maps of energy loss features have been reported.[8,9] Using a retarding field analyzer, Festy and Palmer[8] spectroscopically imaged the surface features on roughened silicon with a sub-50-nm spatial resolution, indicating that it should be possible to provide chemical analysis at these length scales. More recently, Xu et al.[9] used a toroidal detector to map the plasmon loss features of Ag islands on graphite, clearly demonstrating that the Ag islands could be chemically distinguished from the graphite support, but with a limited spatial resolution of 5 μm. Here, we demonstrate elemental contrast in scanning probe energy loss spectroscopy (SPELS) measurements with a spatial resolution of 100 nm by mapping the plasmon response of Ag nanoislands on graphite.

The setup used for these measurements incorporates an Omicron STM-1 scanning tunneling microscope and an electron energy loss spectrometer (LK Technologies), which are housed in an ultrahigh vacuum (UHV) chamber with a base pressure in the low 10^{-10} mbar region. Electrons scattered from the surface are collected by the spectrometer via a series of electrostatic (Einzel) lenses, which are positioned ~6 cm away from the tip–sample junction and tilted at a polar angle of 7° with respect to the sample surface plane. In the spectrometer, the electrons are energy-dispersed in a 127° cylindrical sector analyzer onto a multichannel analyzer (MCA). This detector allows for faster sampling of the energy loss spectrum of the backscattered electrons compared with the SPELS instrument used in previous studies,[5,8,10] which utilized a concentric hemispherical analyzer (CHA) and channeltron. In order to minimize the stray electric fields around the STM junction, the microscope has been modified by incorporating additional electrostatic shielding around the STM tip and the piezo scanner. To facilitate this, the internal op-amp was removed and replaced with a variable gain op-amp (DLPCA-200) located outside the UHV chamber. Highly oriented pyrolytic graphite (HOPG) substrates were cleaved in

air and introduced into UHV via a fast-entry loadlock. Silver films were thermally evaporated onto graphite from a Ta foil crucible containing pieces of 99.99% purity wire. Thin films were deposited at room temperature and subsequently annealed for 10 min at 640 °C to produce large Ag islands with dimensions on the order of hundreds of nanometers. The sample temperature was measured with an infrared pyrometer (Ircon Ultimax UX-20P). STM tips were fabricated from 0.25 mm diameter polycrystalline W wire using a dc electrochemical etch with 2 M NaOH and rinsed with distilled water. The tips were further treated in vacuum by direct heating to remove tungsten oxide.[11,12)]

All measurements were conducted at room temperature. The experimental procedure was as follows. The tip approach to the sample was performed in the field-emission regime using a low field-emission bias (V_{FE}) and current setpoint (I_{FE}). The field-emission current was measured at the sample using a Keithley 485 picoammeter, while the field-emission bias was controlled via the STM controller (Nanonis). The tip could be conditioned by sweeping V_{FE} while the feedback loop was disengaged (i.e., a constant tip–sample separation). Voltage sweeps could also be used to record the dependence of the field-emission current on the bias in order to estimate the tip emission radius using Fowler–Nordheim theory.[13)] Field-emission images of the surface were obtained in constant-current mode. In order to perform SPELS measurements, the field-emission bias and current were increased until a backscattered electron signal was measured at the electron detector. SPELS images were obtained by measuring the energy loss spectrum at each point on a predefined grid in a procedure analogous to current imaging tunneling spectroscopy (CITS). After the SPELS measurements were completed, the tip was withdrawn from the surface, the microscope was switched to operate in the STM mode, and the tip reapproached so that topographic STM images could be obtained for reference. The STM and field-emission images were processed and analyzed using WSxM[14)] and a Python-based SPELS program. Energy loss spectra were recorded over 500 bins (typically 14 meV/bin). During processing, the spectra were smoothed by summing the data over seven neighboring bins. A Gaussian fit was applied to the zero-loss peak, which was then subtracted from the spectrum to yield the plasmon loss peak. Another Gaussian fit was then applied to the plasmon loss peak, the mean value of which was used to identify the plasmon energy. SPELS maps were prepared by integrating the Gaussian fits of the plasmon loss and zero-loss peaks and normalizing the intensity of the loss peak with respect to the elastic peak at each point on the grid map.

The morphology of an as-deposited Ag film is shown in Fig. 1(a). It consists of a continuous layer of metal particles covering the graphite support. Based on STM measurements, the film was determined to have an average thickness of around 40 nm. A SPELS measurement was performed using a 50×50 grid of points covering a $300 \times 300\,nm^2$ area of the film. For the SPELS measurement, the field-emission bias and current were $V_{FE} = 210\,V$ and $I_{FE} = 2.8\,\mu A$, respectively. This resulted in a backscattered electron signal in the range of 4–10 kcps at the electron energy analyzer. The tip was positioned over each grid point for 1.5 s while the backscattered electrons were energy-dispersed and collected. It was not possible to distinguish any elemental contrast in the SPELS image of the as-deposited Ag film as it was continuous. However, the total energy loss spectrum measured over the grid is presented in Fig. 1(b) and shows the Ag plasmon loss peak located at 3.7 eV, which is in good agreement with previous studies.[5,10)] The energy window used for the SPELS measurements was too narrow to observe the graphite π plasmon loss peak at around 6 eV.[4,15,16)]

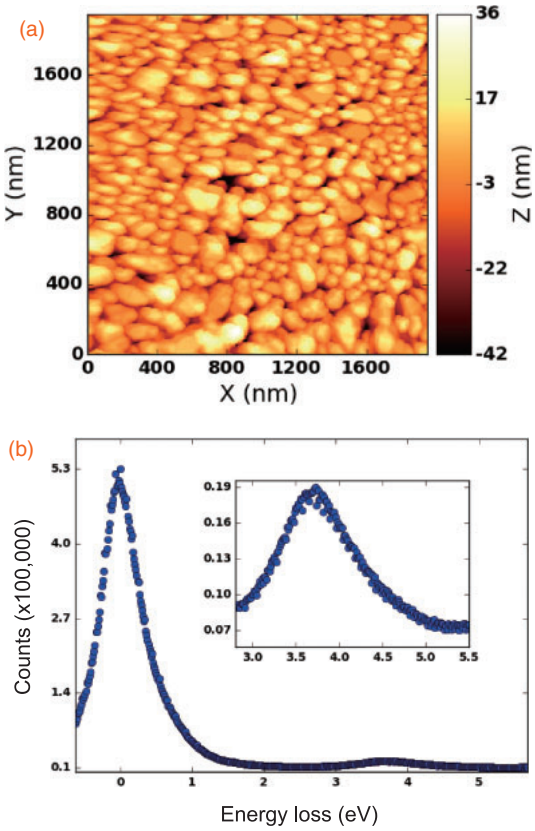

Fig. 1. (a) $1 \times 1\,\mu m^2$ STM image of the as-deposited Ag film taken with $V = 30\,mV$ and $I = 800\,pA$. (b) Energy loss spectrum measured from the as-deposited Ag film with SPELS using $V_{FE} = 210\,V$ and $I_{FE} = 2.8\,\mu A$. The spectrum was obtained by integrating the data measured on a 50×50 grid of points over a $300 \times 300\,nm^2$ area. The inset shows the Ag plasmon loss peak located at 3.7 eV.

In order to produce a sample suitable for SPELS imaging with elemental contrast, the Ag film was annealed at 640 °C for 10 min. This resulted in large Ag nanoislands separated by areas of bare graphite, such as the example shown in the STM image in Fig. 2(a). The lateral dimensions of this nanoisland are on the order of hundreds of nanometers, while it is measured to be $330 \pm 10\,nm$ high by STM. Field-emission images of the nanoisland, which were taken with the same current setpoint as the STM image but using field-emission biases ranging from 30 to 70 V, are presented alongside the STM image in Fig. 2 for comparison. The Ag nanoisland is reasonably well resolved at a low field-emission bias with an island height of $310 \pm 45\,nm$ measured at $V_{FE} = 30\,V$. It is also possible to resolve a 45-nm-high step on the surface of the nanoisland in both Figs. 2(a) and 2(b). However, the lateral and vertical resolutions decrease as the field-emission bias increases owing to the corresponding increase in the tip–sample separation. This is indicated by the change in the tip offset, which is plotted for these STM and field-emission measurements in Fig. 2(e). If the tip–sample separation during the STM measurements is assumed to be

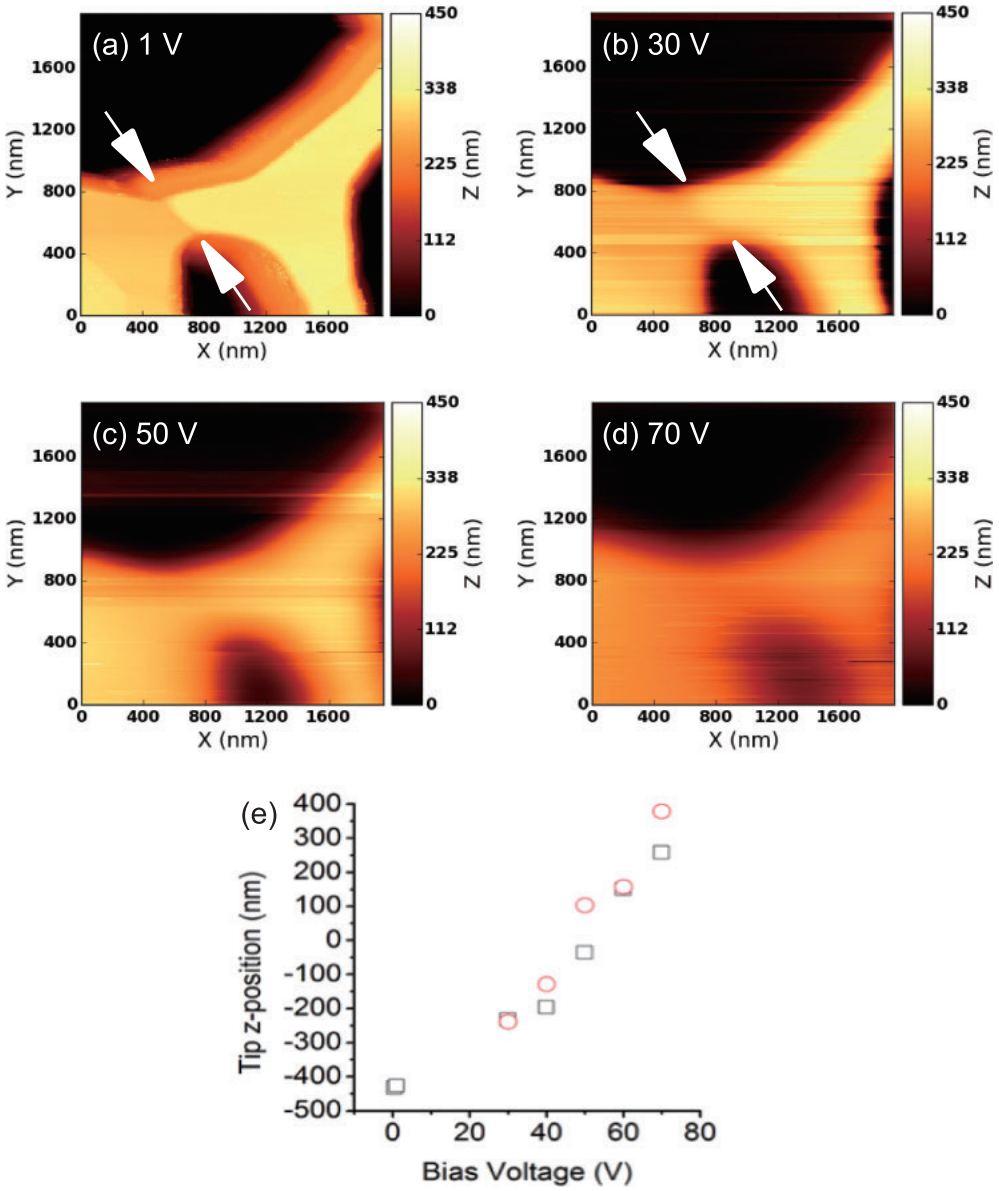

Fig. 2. Topographic images of a Ag nanoisland on graphite taken in both the tunneling and field-emission regimes. (a) STM image taken with a current setpoint of 1 nA and a bias voltage of 1 V. The arrow highlights the position of a step on the surface of the nanoisland. (b–d) Field-emission images taken with the same current setpoint ($I_{FE} = 1$ nA) but with a tip bias of 30, 50, and 70 V, respectively. Each image is composed of 256 × 256 points covering a $2 \times 2\,\mu m^2$ area and has been plane-corrected. (e) Plot of tip offset as a function of the tip bias for different STM and field-emission measurements of the Ag nanoisland shown. Red circles and black squares represent the tip position during two consecutive series of measurements taken in the same area.

around 1 nm, the tip–sample separation during the field-emission measurements can be estimated from Fig. 2(e). It can be seen that the tip–sample separation increases steadily from about 200 nm at $V_{FE} = 30$ V to between 700 and 800 nm at $V_{FE} = 70$ V. It has previously been demonstrated that with a sharp enough tip, it is possible to image monatomic steps in the field-emission mode.[17,18] The beam width of the field-emitted electrons is given by $\Delta x \sim [(R + d) \cdot d]^{1/2}$, where R is the tip emission radius, and d is the tip–sample separation.[17] The emission radius of the tip used in Fig. 2 was estimated to be 160 ± 30 nm based on a Fowler–Nordheim plot of the bias dependence of the field-emission current. The field-emission bias and current setpoint used at the start of the voltage sweep were $V_{FE} = 30$ V and $I_{FE} = 1$ nA, respectively, which from Fig. 2(e), corresponds to a tip–sample separation of 200 ± 30 nm. As a result, the beam width of the field-emitted electrons in Fig. 2(b) is estimated to be 270 ± 30 nm.

An SPELS measurement was performed on the nanoisland shown in Fig. 2 using a field-emission bias of $V = 148$ V and a current setpoint of 5 μA, which resulted in a total backscattered signal measured at the spectrometer of 0.5–2 kcps. Under these conditions, the tip–sample separation was about 650 nm. The same $2 \times 2\,\mu m^2$ area was imaged using a 40 × 40 grid, so that each pixel represents an area of $50 \times 50\,nm^2$. The tip was positioned over each grid point for 10 s while the backscattered electrons were energy-dispersed and collected. Figures 3(a) and 3(b) show the resultant field-emission and backscattered electron images of the Ag nanoisland. The spatial resolution of the backscattered electron image is comparable to that of the simultaneously acquired field-emission image. The total backscattered electron signal measured when the tip was located over the Ag nanoisland was found to be lower than that measured when the tip was over the graphite, so that the Ag nanoisland appears darker

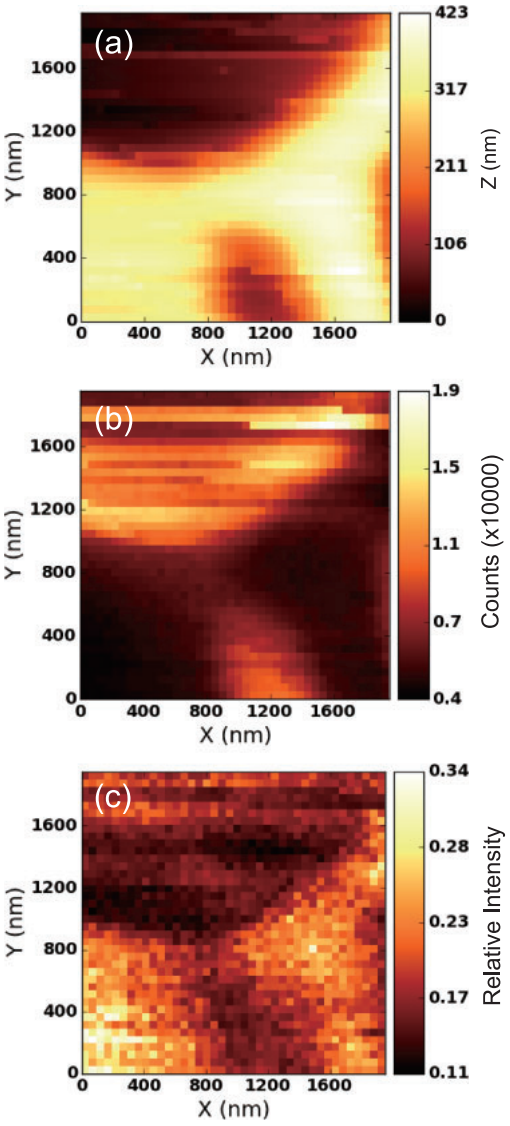

Fig. 3. Simultaneously acquired field-emission, backscattered electron, and normalized plasmon loss images of the same Ag nanoisland on graphite. Each image is composed of a 40×40 grid of points covering a $2 \times 2\,\mu m^2$ area. (a) Field-emission image taken with $V_{FE} = 148\,V$ and $I_{FE} = 5\,\mu A$. (b) Backscattered electron image comprising the total electron signal measured by the analyzer during a 5 s period while the tip is positioned over each grid point. (c) Plasmon loss image obtained by normalizing the Ag plasmon loss peak to the elastic peak at each grid point.

than the support in Fig. 3(b). A similar contrast effect has been recently reported in the near field-emission scanning electron microscopy (NFESEM) measurements of monatomic Fe islands on W(110).[19,20] The material dependence of the low-energy electron reflectivity due to differences in the electronic and crystalline structure is known from low-energy electron microscopy measurements.[21]

While the material contrast is evident in the backscattered electron image, the SPELS measurement allows for unambiguous material identification by means of the energy loss spectrum. In the present case, we focus on the Ag plasmon loss feature at 3.7 eV. In Fig. 3(c), the backscattered electron image is energy-filtered to show the spatial distribution of the normalized Ag plasmon loss feature across the 40×40 measurement grid. The Ag plasmon loss peak was normalized to the zero-loss peak for each point on the grid. Figure 3(c) shows clear contrast between the Ag nanoisland and the graphite support. The relative intensity of the Ag plasmon loss is as high as 34% on top of the Ag nanoisland and decreases to below 17% over the graphite support. A change in contrast is obtained within 1–2 pixels across the island edge, giving a spatial resolution of 50–100 nm. The Ag plasmon response measured when the tip is located over the graphite may be caused by some residual Ag on the graphite, or more likely, because some Ag was transferred to the tip itself. The Ag plasmon response measured on top of the nanoisland is the highest in the lower-left corner of Fig. 3(c), which corresponds to the area of the nanoisland facing closest towards the spectrometer.

In summary, we have performed SPELS measurements using an STM and a cylindrical sector spectrometer. We have demonstrated that by operating the STM in field-emission mode and detecting the energy of backscattered electrons, it is possible to identify element-specific energy loss features, in this case, Ag plasmons, which can be used to provide compositional maps of nanostructures with a spatial resolution of 100 nm. With refinement of the tip and sample preparation, it should be possible to reach a spatial resolution on the order of 10 nm with SPELS. This opens up the prospect of studying the size- and shape-dependent plasmon response of Ag and Au nanostructures, analogous to the type of spatially resolved EELS measurements that are currently only performed using scanning transmission electron microscopy (STEM–EELS).

Acknowledgments The authors gratefully acknowledge the contributions of Scott Holmes and William Terry to the SPELS data analysis. This work was supported financially by the EPSRC.

1) B. Reihl and J. K. Gimzewski, Surf. Sci. **189–190**, 36 (1987).
2) M. Tomitori, H. Terai, and T. Arai, Appl. Surf. Sci. **144–145**, 123 (1999).
3) M. Tomitori, M. Hirade, Y. Suganuma, and T. Arai, Surf. Sci. **493**, 49 (2001).
4) B. J. Eves, F. Festy, K. Svensson, and R. E. Palmer, Appl. Phys. Lett. **77**, 4223 (2000).
5) R. E. Palmer, B. J. Eves, F. Festy, and K. Svensson, Surf. Sci. **502–503**, 224 (2002).
6) Y. Miyatake, T. Nagamura, K. Hattori, Y. Kanemitsu, and H. Daimon, Jpn. J. Appl. Phys. **41**, 4943 (2002).
7) Y. Miyatake, T. Nagamura, K. Hattori, Y. Kanemitsu, and H. Daimon, Jpn. J. Appl. Phys. **42**, 4848 (2003).
8) F. Festy and R. E. Palmer, Appl. Phys. Lett. **85**, 5034 (2004).
9) C. K. Xu, X. J. Chen, X. Zhou, Z. Wei, W. J. Liu, J. W. Li, J. F. Williams, and K. Z. Xu, Rev. Sci. Instrum. **80**, 103705 (2009).
10) A. Pulisciano, S. J. Park, and R. E. Palmer, Appl. Phys. Lett. **93**, 213109 (2008).
11) A.-S. Lucier, H. Mortensen, Y. Sun, and P. Grütter, Phys. Rev. B **72**, 235420 (2005).
12) S. Ernst, S. Wirth, M. Rams, V. Dolocan, and F. Steglich, Sci. Technol. Adv. Mater. **8**, 347 (2007).
13) R. H. Fowler and L. Nordheim, Proc. R. Soc. London, Ser. A **119**, 173 (1928).
14) I. Horcas, R. Fernández, J. M. Gómez-Rodriguez, J. Colchero, J. Gómez-Herrero, and A. M. Baro, Rev. Sci. Instrum. **78**, 013705 (2007).
15) J. Yin, A. Pulisciano, and R. E. Palmer, Small **2**, 744 (2006).
16) J. J. Lawton, A. Pulisciano, and R. E. Palmer, J. Phys.: Condens. Matter **21**, 474206 (2009).
17) J. J. Sáenz and R. García, Appl. Phys. Lett. **65**, 3022 (1994).
18) T. L. Kirk, U. Ramsperger, and D. Pescia, J. Vac. Sci. Technol. B **27**, 152 (2009).
19) D. A. Zanin, M. Erbudak, L. G. De Pietro, H. Cabrera, A. Redmann, A. Fognini, T. Michlmayr, Y. M. Acremann, D. Pescia, and U. Ramsperger, IVNC Tech. Dig., 2013, p. 1.
20) D. A. Zanin, L. G. De Pietro, H. Cabrera, A. Kostanyan, A. Vindigni, D. Pescia, and U. Ramsperger, IVNC Tech. Dig., 2014, p. 141.
21) M. S. Altman, J. Phys.: Condens. Matter **22**, 084017 (2010).